Analysis of a Spectral Difference Scheme with Flux Interpolation on Raviart-Thomas Elements

2 authors:

Georg May
RWTH Aachen University
57 PUBLICATIONS **1,160** CITATIONS
SEE PROFILE

Joachim Schoeberl
TU Wien
166 PUBLICATIONS **4,101** CITATIONS
SEE PROFILE

Aachen Institute for Advanced Study in Computational Engineering Science

Preprint: AICES-2010/04-8

16/April/2010

Analysis of a Spectral Difference Scheme with Flux Interpolation on Raviart-Thomas Elements

G. May, J. Schöberl

RWTH AACHEN UNIVERSITY

AICES

Financial support from the Deutsche Forschungsgemeinschaft (German Research Association) through grant GSC 111 is gratefully acknowledged.

List of AICES technical reports: http://www.aices.rwth-aachen.de/preprints

Analysis of a Spectral Difference Scheme with Flux Interpolation on Raviart-Thomas Elements

Georg May, Joachim Schöberl
April 2010

1 Introduction

High-order numerical schemes that are based on locally discontinuous polynomial approximations on standard unstructured meshes have become quite popular for convection-dominated problems. The Discontinuous Galerkin (DG) method [3, 4] is a well-known example. The Spectral Difference scheme [10, 11, 17] has been proposed as a collocation-based method, using local interpolation of the strong form of the equations, with the aim to achieve superior efficiency by avoiding volume and surface quadratures, while maintaining conservation. The approach extends tensor-product-based collocation approaches that had previously been formulated for quadrilateral meshes [9] to more general unstructured-grid elements.

The Spectral Difference scheme has been found attractive because of its simplicity of formulation and implementation, despite the fact that stability proofs have been only succesful in one dimension [8], while doubts have been raised regarding stability properties on triangles. In fact, it has been found that the scheme is not unconditionally linearly stable in its standard form for triangular grids [16].

In this paper we present and analyze a new formulation of the scheme using an approximation of the divergence operator on Raviart-Thomas (RT) elements. To preserve the purely nodal character of the scheme we use non-standard nodal degrees of freedom in this approximation. By analyzing the eigenvalue spectrum of the spatial operator for the linear periodic problem, we demonstrate the viability of the new formulation, in a similar context where the standard formulation failed [16].

The paper is organized as follows: We recall the formulation of the standard Spectral Difference Scheme, and introduce the alternative approximation of the divergence operator on RT elements in sections 2 and 3, respectively. Section 4 is devoted to analyzing the new formulation. We establish linear stability for a linear periodic model problem with Runge-Kutta time stepping, and provide numerical validation.

2 The Spectral Difference Scheme on Triangles

Consider the scalar hyperbolic conservation law

$$\frac{\partial u(x,t)}{\partial t} + \nabla \cdot f(u) = 0 \,, \tag{1}$$

on some domain $(x,t) \in \Omega \times \mathbb{R}^+$, subject to suitable initial and boundary conditions, where $\Omega \subset \mathbb{R}^2$, and $f(u)$ is a smooth flux function.

Consider a triangulation $\mathcal{T}_h = \{T^{(i)}, i = 1, \ldots, N_T\}$, such that $\overline{\Omega}_h := \bigcup_{i=1}^{N_T} \overline{T^{(i)}}$. Throughout this paper we shall use bracketed superscripts to denote mesh element indices, except where otherwise noted. Assume that there exist mappings $\Phi^{(i)} : \xi \to x$, with nonsingular Jacobian $J^{(i)} = \partial x / \partial \xi$, such that each element in the triangulation can be mapped to a reference domain $T^{(i)} = \Phi^{(i)}(\hat{T})$. Let α be a multi-index, and let $\mathcal{P}_m(\hat{T}) = \text{span}\left\{\xi^\alpha : \xi \in \hat{T}\,, \alpha_i \geq 0\,, |\alpha| \leq m\right\}$ be the space of polynomials of total degree m. Traditionally the Spectral Difference scheme has been derived from the strong form of the governing equations using global interpolants of the numerical solution and the flux function, such that

$$\frac{\partial u_h}{\partial t} + \nabla \cdot f_h(u_h) = 0 \,. \tag{2}$$

The interpolant of the solution u_h is discontinuous across mesh elements, and is defined such that $u_h^{(i)} \in \mathcal{P}_m(\hat{T})$, where $u_h^{(i)} := u_h|_{T^{(i)}} \circ \Phi^{(i)}$ is the numerical solution in element $T^{(i)}$ mapped to the reference domain. The numerical solution may be represented using a standard Lagrange basis,

$$u_h^{(i)} = \sum_{j=1}^{N_m} u_j^{(i)} L_j(\xi) \ , \tag{3}$$

where

$$N_m = \frac{(m+1)(m+2)}{2} \ . \tag{4}$$

The degrees of freedom are thus $u_j^{(i)} = u_h^{(i)}(\xi_j)$, where $\xi_j \in \mathcal{S}_m$, with $\mathcal{S}_m$ a set of interpolation nodes $\mathcal{S}_m = \{\xi_j \, , j = 1, \ldots, N_m\}$ defined on the reference element.

Since it is a necessary condition for optimal order convergence is that the divergence of the flux interpolant f_h be locally a polynomial of degree at least m, it has been standard practice to interpolate each component of the flux function into a polynomial space of degree $m+1$ for each element, such that $\widetilde{f}_h^{(i)} \in [\mathcal{P}_{m+1}(\hat{T})]^2$, where the Piola transform $\widetilde{f}_h^{(i)} := |J^{(i)}|(J^{(i)})^{-1} f_h|_{T^{(i)}}$ is introduced. Using a new set of interpolation nodes $\mathcal{Q}_{m+1} = \{\xi_j \, , j = 1, \ldots, N_{m+1}\}$ with $\mathring{L}_j$ the corresponding Lagrange basis, the local flux reprensentation is written

$$\widetilde{f}_h^{(i)} = \sum_{j=1}^{N_{m+1}} \widetilde{f}_j^{(i)} \mathring{L}_j(\xi) \ , \tag{5}$$

where for $\xi_j \in \mathcal{Q}_{m+1}$ the degrees of freedom are defined as

$$\widetilde{f}_j^{(i)} = \begin{cases} \widetilde{f}(u_j^{(i)}) & , \quad \xi_j \in \hat{T} \\ \widetilde{f}^{num} & , \quad \xi_j \in \partial\hat{T} \end{cases} \ . \tag{6}$$

The coefficients $\widetilde{f}^{num}$ corresponding to $\xi_j \in \partial\hat{T}$ are chosen such that for every element $T^{(l)}$ that shares the node, i.e. $\Phi^{(i)}(\xi_j) = \Phi^{(l)}(\xi_k)$ for some k, one has

$$\widetilde{f}^{num} \cdot \widetilde{n} = h(\widetilde{n}, u_j^{(i)}, u_k^{(l)}) \tag{7}$$

where $\widetilde{n}$ is the transformed outward pointing normal on ∂T, and h is a numerical flux function, which is often chosen in the class of Lipschitz-continuous monotone flux functions [2] for easy incorporation of standard TVD stability theory [6]. This implies that the global interpolant f_h is continuous in normal direction across element interfaces, provided enough degrees of freedom are used on the boundary, i.e. $m+2$ in the present formulation. This is actually the case for popular interpolation nodes of order $m+1$ defined for the triangle, such as Hesthaven's nodes [7] or Fekete points [15]. In more formal nomenclature we have that the global interpolation operator is a mapping into $H(\mathrm{div}; \Omega_h)$, i.e. $f_h \in \{H(\mathrm{div}; \Omega_h) : \widetilde{f}_h^{(i)} \in [\mathcal{P}_{m+1}(\hat{T})]^2\}$.

The scheme may be written in terms of the degrees of freedom as

$$\frac{du_j^{(i)}}{dt} + \frac{1}{|J^{(i)}|}(\nabla^\xi \cdot \widetilde{f}_h^{(i)})(\xi_j) = 0 \ , \qquad j = 1, \ldots N_m \ , \qquad i = 1, \ldots, N_T \ . \tag{8}$$

3 Flux Interpolation Using Raviart-Thomas Elements

Recently, van den Abeele et al. [16] have shown that the scheme described in section 2 is not unconditionally linearly stable for the case $m = 2$. It has even been conjectured that this is true for all order $m \geq 2$. However, using complete polynomial spaces to represent $\widetilde{f}_h^{(i)}$ is not the only way to define interpolation operators into $H(\mathrm{div}; \Omega_h)$. We present a formulation of the Spectral Difference scheme using

Raviart-Thomas elements that is shown to be stable for the linear periodic case, i.e. in the case where the traditional formulation failed.

For the triangular element one defines the Raviart-Thomas space of order m as

$$RT_m = [\mathcal{P}_m]^2 + (x, y)^T \mathcal{P}_m \ . \tag{9}$$

It is known that RT_m is the smallest space having elements with divergence in $\mathcal{P}_m$, see e.g. [1]. Thus, besides the motivation of overcoming stability problems with the standard Spectral Difference scheme, using Raviart-Thomas elements is attractive from the viewpoint of computational cost. Compared to complete polynomial spaces one has $[\mathcal{P}_m]^2 \subset RT_m \subset [\mathcal{P}_{m+1}]^2$. The dimension of RT_m is

$$N_m^{RT} := \dim RT_m = (m+1)(m+3) \ . \tag{10}$$

Taking N_m as defined in eq. (4), we see that in comparison with $[\mathcal{P}_{m+1}]^2$,

$$\Delta_{DOF} = 2N_{m+1} - N_m^{RT} = m + 3 \ . \tag{11}$$

It is evident that, while the relative difference is asymptotically negligible (both spaces have dimensionality increasing with m^2), for fixed intermediate orders it can be significant. A few examples for polynomial orders of practical interst are given in Table 1.

m	RT_m	$[\mathcal{P}_{m+1}]^2$	Δ_{DOF}
1	8	12	4
2	15	20	5
3	24	30	6
4	35	42	7

Table 1: Total number of degrees of freedom for RT_m and $[\mathcal{P}_{m+1}]^2$ elements.

Here we define the degrees of freedom so as to preserve the nodal character of the Spectral Difference Scheme. To this end we define a set of interpolation nodes and vectors as $\mathcal{R}_m = \left\{(\xi_i, s_i); i = 1, \ldots, N_m^{RT}\right\}$, where $\xi_i \in \hat{T}$, and $s_i \in \mathbb{R}^2$ is a unit vector. Globally, we thus look for a projection onto $\mathcal{W}_h = \{q_h \in H(\mathrm{div}; \Omega_h) : \widetilde{q}_h^{(i)} \in RT_m\}$ such that

$$\widetilde{q}_h^{(i)} = \sum_{k=1}^{N_m^{RT}} c_k \psi_k \ , \tag{12}$$

where $\psi_k \in RT_m$ are basis functions with property $\psi_k(\xi_j) \cdot s_j = \delta_{jk}$ for all $(\xi_j, s_j) \in \mathcal{R}_m$, and $c_k = \widetilde{q}^{(i)}(\xi_k) \cdot s_k$. In the context of conservation laws, the flux projection of eq. (5) is thus re-written

$$\widetilde{f}_h^{(i)} = \sum_{k=1}^{N_m^{RT}} \widetilde{f}_{s,k}^{(i)} \psi_k \ , \tag{13}$$

where

$$\widetilde{f}_{s,k}^{(i)} = \begin{cases} \widetilde{f}(u_k^{(i)}) \cdot s_k & , \quad \xi_k \in \hat{T} \\ h(\widetilde{n}_k, \cdot, \cdot) & , \quad \xi_k \in \partial\hat{T} \end{cases} \ . \tag{14}$$

Note that here the coeffcients are scalar, and the basis functions are vector-valued, in direct opposition of eq. (5). Furthermore, in the standard approach numerical fluxes are not used directly, but are computed to replace the normal projection of the analytical fluxes at boundaries (cf. eqns. (6) and (7)). In the new approach numerical fluxes can be used directly for degrees of freedom on the boundary. With this new definition of the flux interpolant the Spectral Difference Scheme, eq. (8), remains formally unchanged.

We denote this scheme RT_m-based Spectral Difference to highlight the novel flux representation. Note, however, that the solution representation is still given by eq. (3), i.e. a standard Lagrange basis in $\mathcal{P}_m$.

The choice of interpolation nodes ξ_k and directions s_k is not a priori clear. We have not attempted to optimize node placement according to interpolation properties, but we show in section 4, that linear stability may depend on this choice. From standard theory it is clear that the RT_m element has $m+1$ degrees of freedom on each edge, and $2N_{m-1}$ degrees of freedom in the interior [1]. In the present paper we use N_{m-1} points in the interior, each with two orthogonal unit vectors. Figure 1 shows examples of RT elements of orders 1 through 3, where points on the boundary have been placed at Gauss-Legendre

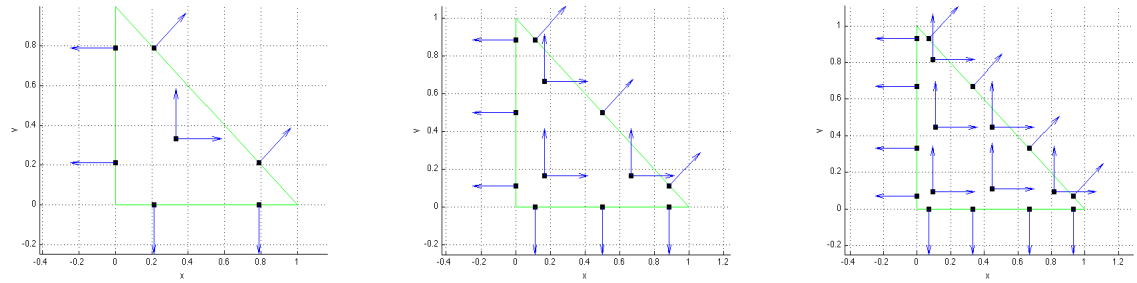

(a) RT_1 Element (b) RT_2 Element (c) RT_3 Element

Figure 1: RT_m elements: Examples of Raviart-Thomas elements of order m.

integration points, and interior points have been placed at high-order quadrature points for the triangle. These points will be specified in section 4, where it is demonstrated that at least the selection of interior points can be informed by linear stability considerations.

The degrees of freedom on the boundary determine how many numerical fluxes need to be computed for interior elements. The cost of numerical flux computations is much higher than analytical flux evaluation, even taking into account that one numerical flux can be used for two elements that share the edge node. There are $m+1$ nodes on the boundary for RT_m elements, while for the standard Spectral Difference scheme most popular interpolation nodes for $\mathcal{P}_{m+1}$, such as Hesthaven's nodes [7] or Fekete points [15], have $m+2$ points on the boundary, which are actually the Chebyshev-Lobatto nodes of corresponding order. In any case, the difference between RT_m elements and $[\mathcal{P}_{m+1}]^2$ elements is a fixed number, independent of m.

4 Eigenvalue Analysis for a Linear Periodic Problem

We consider the linear advection problem

$$\frac{\partial u}{\partial t} + V \cdot \nabla u = 0 \ , \tag{15}$$

where $V = ||V||(\cos\theta, \sin\theta)$ is the (constant) advection velocity, with periodic initial and boundary condition on some square domain, say $\Omega = [0,1]^2$.

4.1 The Spectrum of the Discrete Advection Operator

We treat the problem by considering a Cartesian mesh with each mesh element decomposed into two triangles. We formulate the Spectral Difference Scheme for the triangles by considering the joint operator for every two triangles that form a quadrilateral mesh element, to which we assign a standard structured-mesh index tuple (i,j). For $\theta \in [0, \pi/2]$, if upwind fluxes are used on element boundaries, the semi-discrete

Spectral Difference Scheme may be written

$$\Delta t\, \dot{\mathbf{u}}^{(i,j)} = -\nu \left(A\mathbf{u}^{(i,j)} + B\mathbf{u}^{(i-1,j)} + C\mathbf{u}^{(i,j-1)} \right) , \tag{16}$$

where the CFL number is given by

$$\nu = \frac{||V||\Delta t}{h} , \tag{17}$$

and $\mathbf{u}^{(i,j)} = (u_1^{(i,j)}, \ldots, u_{N_m}^{(i,j)}, u_{N_m+1}^{(i,j)}, \ldots, u_{2N_m}^{(i,j)})^T$ collects all the degrees of freedom for the two triangular cells that make up the quadrilateral mesh element (i,j). The matrices in eq. (16) follow in a straightforward calculation from the concatenated application of a reconstruction operation, used to evaluate $u_h^{(i)}$ at the flux collocation nodes, and a differentiation operation, evaluating the divergence of $\widetilde{f}_h^{(i)}$, using upwind fluxes, at the solution nodes. The factor h contained in the cfl number (17) is the (constant) edge length of the fused quad meshes. Formulation (16) is independent of the choice of reference element for linear mappings.

Applying Fourier analysis and considering a particular mode $\hat{\mathbf{u}} e^{\hat{\imath}\mathbf{k}\cdot\mathbf{x}}$ the scheme becomes

$$\Delta t \frac{d\hat{\mathbf{u}}}{dt} = \nu Z \hat{\mathbf{u}} , \tag{18}$$

where ν is the CFL number, and $Z \in \mathbb{C}^{N_m \times N_m}$ is the Fourier Symbol of the spatial discretization,

$$Z = -\left(A + Be^{-\hat{\imath}\xi} + Ce^{-\hat{\imath}\eta} \right) \tag{19}$$

where the grid frequency $(\xi, \eta) := (k_x h, k_y h)$ has been defined. The eigenvalues λ are evaluated numerically at discrete grid frequencies $(\xi_k, \eta_k) \in [0, 2\pi]^2$, i.e. $\lambda = \lambda(\xi_k, \eta_k)$. We have made sure to use sufficiently many grid frequencies so that the results are 'grid converged'. We denote the spectrum of the Fourier Symbol by $\sigma(Z)$, and the spectral radius by $\rho(Z)$.

4.1.1 Placement of Boundary Nodes

Let ζ be a parametrization of the edge, such that $\zeta \in [-1, 1]$. Furthermore, let ζ_i^{LG} denote Legendre-Gauss quadrature points. We scale the point placement on edges by a parameter $\alpha \in (0, 1]$, such that

$$\zeta_i = \zeta_i^{LG} \frac{\alpha}{\max_{1 \le i \le m+1} |\zeta_i^{LG}|} , \qquad i = 1, \ldots, m+1 . \tag{20}$$

This scales the node placement such that for $\alpha = 1$ the edge endpoints are included, and for $\alpha = 0$ the points collapse on the edge mid-points. Obviously the latter case leads to a singular stencil.

Both the spectral radius $\rho(Z)$, and the maximum real part of the spectum $\max_{\xi,\eta}(Re(\lambda(\xi, \eta)))$ do *not* depend on α for all schemes tested here, i.e. $m = 1, 2, 3$. Of course not all interesting node placements are obtained in this manner (e.g. Chebyshev-Lobatto nodes are not obtained from the Gaussian integration points by this simple scaling). However, the α-independence of the spectrum strongly suggests that placement of edge nodes does not affect linear stability, so that other considerations, such as interpolation properties or efficiency, should determine this choice. We have not attempted to optimize interpolation properties, as we are only concerned with linear stability here, but it is clear that including the endpoints of the edge may save reconstruction cost and function evaluations for nonlinear schemes, as cell vertices are always shared by two edges.

4.1.2 Placement of Interior Nodes

For RT_1 flux interpolation, there are two interior degrees of freedom, which we both put in the centroid of the triangle, and use x- and y-directional unit vectors for the interpolation, see Figure 1(a). Due to symmetry considerations we do not vary this point placement.

For the RT_2 element there are six interior degrees of freedom, i.e. three points, each with x and y unit vectors. Again due to symmetry there is one degree of freedom in the placement of these nodes. Let the vertices of the reference element be denoted by $\xi_1^v, \xi_2^v, \xi_3^v$, and introduce a parameter $\alpha \in (0,1)$, such that the interior points $\xi \in \hat{T}$ are scaled as

$$\xi_i = \xi_i^v + \alpha(\xi^c - \xi_i^v) \ , \qquad i = 1,2,3 \ , \tag{21}$$

where ξ^c is the centroid of the reference element. For $\alpha = 0$ the points remain at the corners, while for $\alpha = 1$ they collapse at the centroid. Both these extreme choices lead to a singular stencil [1]. Here one can give a clear indication on what is the best point placement regarding linear stability. Figure 2 summarizes the eigenvalue analysis. More specifically, for $\alpha < 0.5$ the eigenvalues have positive real parts,

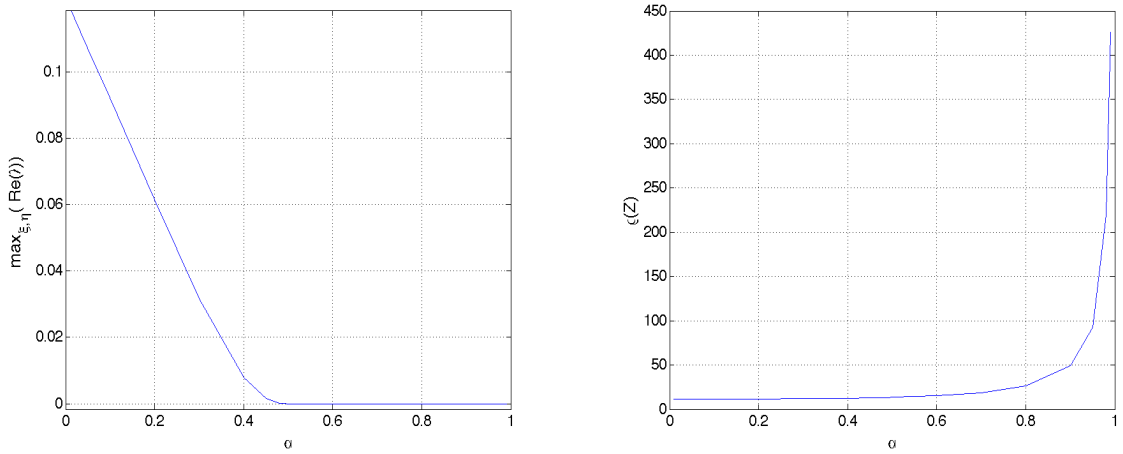

(a) $\max_{\xi,\eta} Re(\lambda(\xi,\eta))$ as a function of the scaling parameter α.

(b) $\max_{\xi,\eta} \rho(Z(\xi,\eta))$ as a function of the scaling parameter α.

Figure 2: Influence of the scaling parameter α for interior collocation nodes on the spectrum of the Fourier Symbol Z for the Spectral Difference scheme using RT_2 elements for flux representation.

see figure 2(a), which we reject from linear stability considerations [2]. Furthermore we see in Figure 2(b) that the spectral radius is monotonically increasing with α, which implies that the smallest value of α having eigenvalues with non-positive real parts is optimal from a linear stability viewpoint. Thus one ought to choose $\alpha = 0.5$. Interestingly enough this optimal choice corresponds to using high-order integration nodes in the interior of triangles: The points obtained have area coordinates $l_1 = l_2 = 1/6$, which leads to an integration rule with weights $w_i = 1/3$, exact for polynomials of total degree 2. (There are no higher order three-point rules).

For the case of RT_3 there are six interior points each with two unit vectors. Consider six points at the element boundaries, three at corner points, and three at edge midpoints, and again use eq. (21). Figure 3 reveals that none of the nodes obtained in this way are stable. The maximum real part of the eigenvalues as a function of α is always positive. However, vaying α is not the only parameter choice. Motivated by the results from the RT_2 case, we use the six-point high-order quadrature rule shown in Table 2. This rule is accurate for polynomials of total degree 4, the maximum known for six-point quadrature rules. Indeed the eigenvalues based on these nodes have non-positive real parts.

[1] This may not be obvious for the case $\alpha = 0$. Recall that there are already $m+1$ degrees of freedom on each edge. If the interior points are placed at the element vertices, all the degrees of freedom are on the boundary, and the stencil becomes singular.

[2] While some time stepping schemes have stability regions that include small parts of the right-half plane, we do not consider this generally viable.

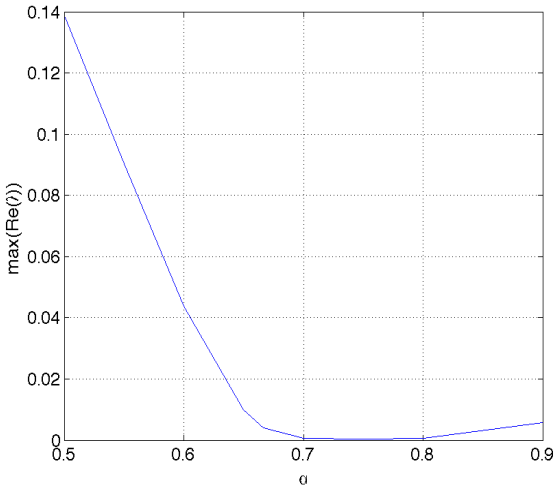

Figure 3: Influence of the scaling parameter α for interior collocation nodes on the spectrum of the Fourier Symbol Z for the Spectral Difference scheme using RT_3 elements for flux representation.

Table 2: Six-point quadrature rule of order 4 in area coordinates, cf. [5, 12]

l_1	l_2	w
0.816847572980459	0.091576213509771	0.109951743655322
0.108103018168070	0.445948490915965	0.223381589678011

Figure 4 shows results for RT_m elements identified as optimal for linear stability. With these choices no positive real parts are present in the spectrum of the operators, unlike the $[\mathcal{P}_m]^2$-based Spectral Difference discretization for triangles [16]. We demonstrate below that permissible CFL numbers based on numerical evaluation of the spectrum can be verified in numerical experiments, and thus lend some credibility to the assertion that this formulation of the Spectral Difference scheme is indeed linearly L_2-stable.

4.1.3 Linear Stability with Multistage Schemes

Once the Fourier symbol of the advection operator is known one may extend the analysis to a time stepping scheme to establish full discrete stability and permissible CFL numbers. Ultimately one aims to find the amplification factor $G(\nu;\xi,\eta)$, such that $\hat{\mathbf{u}}(t^{n+1}) = G\hat{\mathbf{u}}(t^n)$, the exact form of which depends on the Fourier symbol Z and the time discretization of (18). In this section we consider, following [13], multistage schemes of the type

$$\begin{aligned} \hat{\mathbf{u}}^{(0)} &= \hat{\mathbf{u}}(t^n) \ , \\ \hat{\mathbf{u}}^{(k)} &= \sum_{l=0}^{k-1} \alpha_{kl}\hat{\mathbf{u}}^{(l)} + \nu\beta_{kl}Z\hat{\mathbf{u}}^{(l)} \ , \qquad k = 1, \ldots, M \ , \\ \hat{\mathbf{u}}(t^{n+1}) &= \hat{\mathbf{u}}^{(M)} \ . \end{aligned} \tag{22}$$

For the intermediate amplification factor $\hat{\mathbf{u}}^{(k)} = G^{(k)}\hat{\mathbf{u}}^{(0)}$ one obtains by induction

$$G^{(0)} = I \ , \qquad G^{(k)} = \sum_{l=0}^{k-1} \left(\alpha_{kl}I + \beta_{kl}\nu Z\right) G^{(l)} \ . \tag{23}$$

Setting $k = M$ gives the amplification factor for the update from time level t^n to t^{n+1}. One needs to compute the eigenvalues of the amplification factor, noting that for diagonalizable G, it is sufficient for L_2-Stability that

$$\rho(G(\nu;\xi,\eta)) \leq 1 \ , \qquad \forall \ (\xi,\eta) \ \in [0,2\pi]^2 \ , \tag{24}$$

which is thus formulated as a condition on ν. The analytical evaluation of Eq. (24) as a function of ν and (ξ,η) becomes extremely complicated for higher orders of accuracy, but can be easily accomplished numerically. We have used Shu's three-stage scheme [14] in eq. (22). The coefficients of the scheme may be written, arranged in matrix form, as

$$\alpha = \begin{pmatrix} 1 & & \\ \frac{3}{4} & \frac{1}{4} & \\ \frac{1}{3} & 0 & \frac{2}{3} \end{pmatrix} \ , \qquad \beta = \begin{pmatrix} 1 & & \\ 0 & \frac{1}{4} & \\ 0 & 0 & \frac{2}{3} \end{pmatrix} \ . \tag{25}$$

Again we have made sure to include sufficiently many discrete frequencies to obtain grid-converged results. Table 3 shows numerically computed CFL numbers for the two-dimensional linear advection problem (15) for several advection angles $0 \leq \theta \leq \pi/2$.

4.2 Convergence Study

In order to verify the accuracy of the scheme for the linear problem (15), a convergence study has been conducted. We used periodic boundary conditions for $(x,y) \in [0,1]^2$, and initial conditions $u(x,y) = \sin(2\pi(x+y))$. Results for the RT_m-based Spectral Difference schemes for $m = 1,2,3$ are summarized in Tables 4 thorugh 6. It may be seen that the optimal order of accuracy, i.e. $m+1$ has been reached for all schemes. Figure 5 shows a graphical view of the convergence properties.

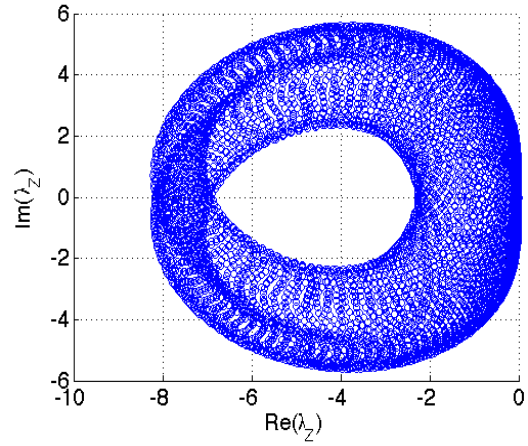

(a) $\sigma(Z)$ for $m = 1$ and $\theta = \pi/8$

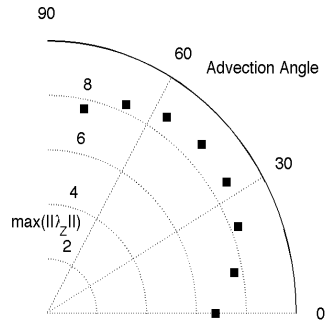

(b) $\max_{\xi,\eta} \rho(Z)$ for $k = 1$ and $0 \leq \theta \leq \pi/2$

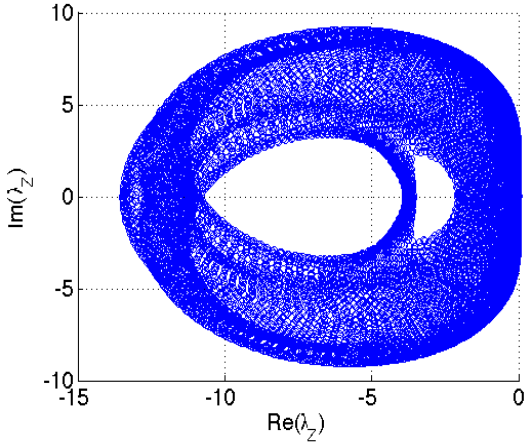

(c) $\sigma(Z)$ for $m = 2$ and $\theta = \pi/8$

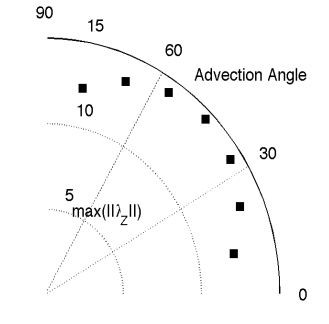

(d) $\max_{\xi,\eta} \rho(Z)$ for $k = 2$ and $0 \leq \theta \leq \pi/2$

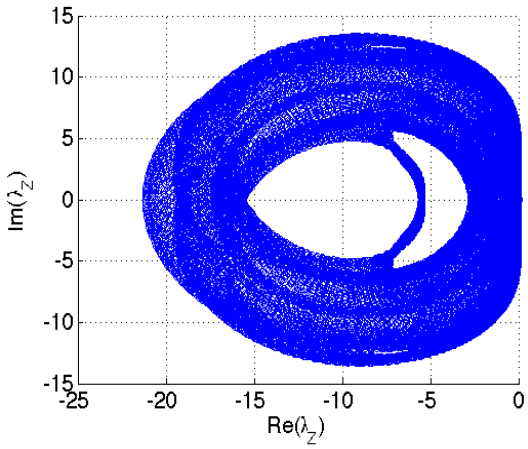

(e) $\sigma(Z)$ for $m = 3$ and $\theta = \pi/8$

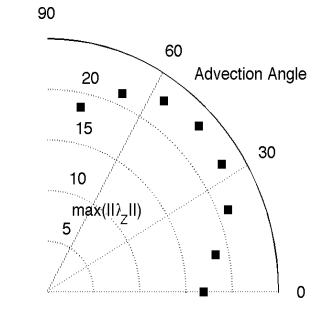

(f) $\max_{\xi,\eta} \rho(Z)$ for $k = 3$ and $0 \leq \theta \leq \pi/2$

Figure 4: Spectrum of the Fourier symbol Z for the Spectral Difference scheme with flux interpolation on RT_m elements. Left: scatter plot of $\sigma(Z(\xi, \eta))$ for discrete grid frequencies $(\xi, \eta) \in [0, 2\pi]^2$, and advection angle $\theta = \pi/8$. Right: $\max_{\xi,\eta} \rho(Z(\xi, \eta))$ as a function of advection angle θ.

Table 3: Permisible CFL numbers for the linear advection equation with periodic boundary conditions for several advection angles $0 \leq \theta \leq \pi/2$. Note for $\theta > \pi/4$ one has $\mathrm{CFL}_\theta = \mathrm{CFL}_{\pi/2-\theta}$, due to symmetry, so that only values for $\theta \leq \pi/4$ are tabulated.

	CFL		
k	$\theta = 0$	$\theta = \pi/8$	$\theta = \pi/4$
1	0.352	0.289	0.281
2	0.215	0.182	0.172
3	0.140	0.118	0.108

Table 4: Convergence of RT_1-based Spectral Difference scheme

# Elements	L_∞(Error)	Order	L_2(Error)	Order
10	8.641900e-02		7.610900e-0	
20	2.312800e-02	1.901708e+00	2.011200e-02	1.920011e+00
50	3.777500e-03	1.977518e+00	3.239600e-03	1.992672e+00
100	9.465000e-04	1.996757e+00	8.093300e-04	2.001016e+00
200	2.366000e-04	2.000152e+00	2.021900e-04	2.001016e+00
500	3.784900e-05	2.000202e+00	3.233400e-05	2.000553e+00
1000	9.461300e-06	2.000145e+00	8.081900e-06	2.000286e+00

Table 5: Convergence of RT_2-based Spectral Difference scheme

# Elements	L_∞(Error)	Order	L_2(Error)	Order
10	1.110400e-02		1.040400e-02	
20	1.406800e-03	2.980590e+00	1.262800e-03	3.042440e+00
50	9.017500e-05	2.998307e+00	8.122900e-05	2.994480e+00
100	1.130600e-05	2.995639e+00	1.017700e-05	2.996683e+00
200	1.414600e-06	2.998623e+00	1.273100e-06	2.998895e+00
500	9.057400e-08	2.999523e+00	8.151200e-08	2.999550e+00
1000	1.132300e-08	2.999841e+00	1.019100e-08	2.999717e+00

Table 6: Convergence of RT_3-based Spectral Difference scheme

# Elements	L_∞(Error)	Order	L_2(Error)	Order
10	5.871900e-04		5.230400e-04	
20	4.784800e-05	3.617297e+00	4.068600e-05	3.684317e+00
50	1.069100e-06	4.148478e+00	8.931700e-07	4.167741e+00
100	6.609000e-08	4.015821e+00	5.498300e-08	4.021877e+00
200	4.108400e-09	4.007783e+00	3.417000e-09	4.008183e+00
500	1.056700e-10	3.994876e+00	8.803200e-11	3.993075e+00
1000	7.683900e-12	3.781583e+00	7.493600e-12	3.554297e+00

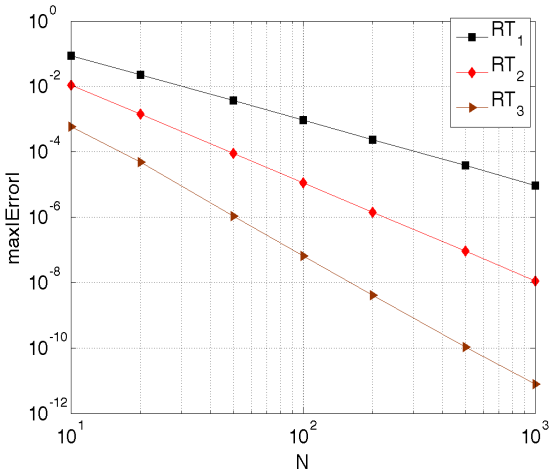

Figure 5: Convergence of RT_m-based Spectral Difference Scheme for the linear advection equation, for $m = 1, 2, 3$ on an $N \times N$ mesh. Total number of triangles is thus $2N^2$.

References

[1] Franco Brezzi and Michel Fortin. *Mixed and Hybrid Finite Element Methods*, volume 15 of *Springer Series in Computational Mathematics*. Springer-Verlag, 1991.

[2] B. Cockburn and C. W. Shu. TVB Runge-Kutta local projection Discontinuous Galerkin finite element method for conservation laws II: General framework. *Math. Comp.*, 52(186):411–435, 1988.

[3] B. Cockburn and C. W. Shu. Runge-Kutta Discontinuous Galerkin methods for convection-dominated problems. *J. Sci. Comp.*, 16(3):173–261, 2001.

[4] Bernardo Cockburn, George Em Karniadakis, and Chi-Wang Shu. The development of Discontinuous Galerkin methods. In Bernardo Cockburn, George Em Karniadakis, and Chi-Wang Shu, editors, *Discontinuous Galerkin Methods: Theory, Computation and Applications*, volume 11 of *Lecture Notes in Computational Science and Engineering*, pages 3–50. Springer, 2000.

[5] G. R. Cowper. Gaussian quadrature formulas for triangles. *Int. J. Numer. Meth. Eng.*, 7(3):405–408, 1973.

[6] A. Harten. High-resolution schemes for hyperbolic conservation laws. *J. Comp. Phys.*, 49(3):357–393, 1983.

[7] J. S. Hesthaven. From electrostatics to almost optimal nodal sets for polynomial interpolation in a simplex. *SIAM J. Num. Anal.*, 35(2):655–676, 1998.

[8] Antony Jameson. A proof of the stability of the spectral difference method for all orders of accuracy. *J. Sci. Comput.*, DOI 10.1007/s10915-009-9339-4 2009.

[9] D. A. Kopriva and J. H. Kolias. A conservative staggered-grid Chebyshev multidomain method for compressible flows. *J. Comp. Phys.*, 125:244–261, 1996.

[10] Y. Liu, M. Vinokur, and Z. J. Wang. Discontinuous spectral difference method for conservation laws on unstructured grids. In *Proceedings of the 3rd International Conference on Computational Fluid Dynamics, July 12-16, 2004, Toronto, Canada*. Springer, 2004.

[11] Y. Liu, M. Vinokur, and Z. J. Wang. Spectral Difference method for unstructured grids I: Basic formulation. *J. Comp. Phys.*, 216(2):780–801, 2006.

[12] J. N. Lyness and D. Jespersen. Moderate degree symmetric quadrature rules for the triangle. *IMA Journal of Applied Mathematics*, 15(1):19–32, 2 1975.

[13] G. May. *A Kinetic Scheme for the Navier-Stokes Equations and High-Order Methods for Hyperbolic Conservation Laws*. PhD thesis, Stanford University, Stanford, CA 94305, 2006.

[14] C.-W. Shu and S. Osher. Efficient implementation of essentially non-oscillatory shock capturing schemes. *J. Comp. Phys.*, 77:439–471, 1988.

[15] M. A. Taylor, B. A. Wingate, and R. E. Vincent. An algorithm for computing Fekete points in the triangle. *SIAM J. Numer. Anal.*, 38(5):1707–1720, 2000.

[16] K. van den Abeele, C. Lacor, and Z. J. Wang. On the stability and accuracy of the spectral difference method. *J. Sci. Comput.*, 37(2):162–188, 2008.

[17] Z. J. Wang, Y. Liu, G. May, and A. Jameson. Spectral Difference method for unstructured grids II: Extension to the Euler equations. *J. Sci. Comput.*, 32(1):54–71, 2007.